Available online at www.sciencedirect.com
ScienceDirect
Progress in Oceanography 74 (2007) 252–272
Progress in Oceanography
www.elsevier.com/locate/pocean

Analysis of mixing and biogeochemical effects induced by tides on the Atlantic–Mediterranean flow in the Strait of Gibraltar through a physical–biological coupled model

D. Macías [a,*], A.P. Martin [b], J. García-Lafuente [c], C.M. García [a], A. Yool [b], M. Bruno [d], A. Vázquez-Escobar [d], A. Izquierdo [d], D.V. Sein [e], F. Echevarría [a,f]

[a] *Departamento de Biología, Área de Ecología, Facultad de Ciencias del Mar y Ambientales, Universidad de Cádiz, CASEM. Avda. República Saharaui s/n., 11510 Puerto Real, Cádiz, Spain*
[b] *National Oceanography Centre, Southampton, SO14 3ZH, UK*
[c] *Departamento de Física Aplicada II, Campus de Teatinos, Universidad de Málaga, 29071 Málaga, Spain*
[d] *Departamento de Física Aplicada, Facultad de Ciencias del Mar y Ambientales, Universidad de Cádiz, 11510 Puerto Real, Cádiz, Spain*
[e] *Alfred Wegener Institute for Polar and Marine Research, Bussestrasse 24, D-27570 Bremerhaven, Germany*
[f] *Centro Andaluz de Ciencia y Tecnología Marina, 11510 Puerto Real, Cádiz, Spain*

Available online 14 April 2007

Abstract

The output of a two-layer hydrodynamic model along a west–east section of the Gibraltar Strait is used to estimate tidal induced mixing between the Mediterranean and Atlantic water layers and to simulate the effects of mixing processes on biogeochemical fluxes and the pelagic community of the area. The hydrodynamic model is used to estimate interfacial mixing and water advection which drive the dynamics of the pelagic community. The model was run for 13 months, in order to analyse the effect of annual modulations in tidal amplitude on mixing. Incorporation of a third intermediate layer leads to a significant improvement in the model results, showing the necessity for a three layer circulation scheme when modelling biogeochemical processes in the Strait of Gibraltar. Pelagic processes are modelled using a simple Nutrient–Phytoplankton–Zooplankton (NPZ) model. The intense physical mixing and advection in the channel are the main influence on plankton dynamics in the area. It is found that residence times within the channel are so short that phytoplankton communities cannot grow appreciably during their transit. As a consequence, the use of a more sophisticated biogeochemical model does not lead to significant changes in the results obtained. According to the model, mixing over the Camarinal Sill causes an average of 16% of the out-flowing nutrients to be returned back to the Mediterranean. This fraction varies between 4% and 35% as a function of the tidal amplitude. The comparison of the model results with field data suggests that in order to obtain an accurate simulation of the plankton ecosystem dynamics in the strait, it is necessary to take into account the full horizontal flow, as recirculation and coast-channel interactions seems to be very important processes in explaining the biological patterns in the area.

Keywords: Spain; Strait of Gibraltar; Coupled models; Mixing processes; Tides; Tidal mixing; Internal waves; Patchiness

* Corresponding author. Tel.: +34 956 016025; fax: +34 956 016019.
E-mail address: diego.macias@uca.es (D. Macías).

0079-6611/$ - see front matter © 2007 Elsevier Ltd. All rights reserved.
doi:10.1016/j.pocean.2007.04.006

1. Introduction

The negative hydrological budget of the Mediterranean Sea as a whole creates the well-known inverse estuarine circulation through the Strait of Gibraltar (Lacombe and Richez, 1982; Armi and Farmer, 1988; Hopkins, 1999) that leads to a natural tendency to oligotrophy in the Mediterranean basin. The Strait plays a critical role in this hydrological budget and, along with the climatic conditions over the Mediterranean area, determines the size and structure of the exchanged flows (Bryden and Kinder, 1991; García Lafuente and Criado Aldeanueva, 2001). The nutrient budget of the Mediterranean Sea depends on the water exchange through the Strait of Gibraltar, as well as on atmospheric and river inputs (Béthoux et al., 1998). It is, therefore, expected that the flow dynamics and mixing in the Strait of Gibraltar play a non-negligible role in the nutrient budget of the Mediterranean basin (Packard et al., 1988; Minas et al., 1991).

Over annual timescales the water exchange through the Strait of Gibraltar can be regarded as a nearly constant inflow of Atlantic waters towards the Mediterranean in the upper layer and a nearly constant outflow of deep Mediterranean waters towards the Atlantic beneath. The magnitude of these virtually regular flows has been estimated by direct measurement (e.g., Bryden and Kinder, 1988; Pettigrew, 1989; Bryden et al., 1994; García-Lafuente et al., 2000; Tsimplis and Bryden, 2000) and by numerical models (Wu and Haines, 1996; Sein et al., 1998; Hopkins, 1999; Sannino et al., 2002). Although the reported values differ from each other, a reasonable value of general agreement is around 0.8 Sv ($1\ \mathrm{Sv} = 1 \times 10^6\ \mathrm{m^3/s}$), the inflow being around 5% greater than the outflow in order to compensate for evaporative losses in the Mediterranean Sea. The recent study by Basheck et al. (2001), who calculated an Atlantic inflow of 0.81 Sv and a Mediterranean outflow of 0.76 Sv from field observations corrected by an inverse tidal model, is within the range of observations and it will be used as a reference in this manuscript. The nutrient concentration of the exchanged waters is estimated as 1.2 mmol N/m^3 in the inflowing Atlantic waters and 9.6 mmol N/m^3 in the outflowing Mediterranean waters (Gómez et al., 2000b; Minas et al., 1991; Dafner et al., 2003). With these concentrations and using the flow estimates of Basheck et al. (2001), the nutrient fluxes towards the Mediterranean Sea and towards the Atlantic Ocean would be 972 and 7296 mol N/s, respectively. Thus, the Mediterranean Sea would export a net amount of 6324 mol N/s (or 2914 ton N/year) to the Atlantic ocean through the Strait of Gibraltar.

The long-term average pattern depicted above exhibits large fluctuations at different time scales. Seasonal and subinertial (meteorologically-induced) fluctuations of, typically, 0.1 Sv and 0.5 Sv, respectively (Candela, 1990; García-Lafuente et al., 2002) have been reported, but the main source of variability is tidal. Tidal currents produce flow fluctuations whose amplitude can be up to 4 Sv during spring tides, more than four times greater in magnitude than the time-averaged flow (García-Lafuente and Vargas Domínguez, 2003). An interesting and curious fact first pointed out by Bryden et al. (1994) is that tides contribute to the mean exchange through the positive correlations between the position of the interface separating Mediterranean and Atlantic waters (AMI hereinafter) and the strength of the tidal currents. Bryden et al. (1994) showed that, on average, almost half of the flow exchange measured in the main sill of Camarinal, in the western side of the Strait (see Fig. 1), occurs by virtue of this correlation. The analysis of Vargas et al. (2006) confirmed this mechanism (which they named tidal-rectification of flows) but they went further and showed that tidal rectification dominates the exchange during spring tides and was negligible during neap tides. The question remains open as to whether or not the exchange of other substances also follows a pulsating pattern related to the fortnightly cycle of tides, an issue that becomes more complex if mixing is taken into account.

The bottom topography changes dramatically from 900 to 300 m depth near the Camarinal Sill (Fig. 1). The interaction between flows and this sharp topography makes the AMI change position abruptly too. This is particularly true during certain phases of the tidal cycle when the abrupt changes of the AMI are related either to the formation of internal hydraulic jumps (Boyce, 1975; Armi and Farmer, 1985; Garrett et al., 1990), a phenomenon that prevails during moderate to strong (spring) tides, or arrested internal waves (Bruno et al., 2002), which are more usual during weak (neap) tides. Such undulatory processes enhance interfacial mixing (Wesson and Gregg, 1994) and can inject deep, nutrient-rich water into the upper layer of Atlantic water. The upwelled inorganic nutrients are advected towards the Mediterranean Sea in the upper layer enhancing the primary production in the Alboran Sea to the east of the Strait. The turbulence-favouring abrupt nature of hydraulic jumps relative to the smoother arrested waves suggests a fortnightly cycle for mixing and, hence, for the exchange of dissolved substances. The simultaneous occurrence of enhanced mixing

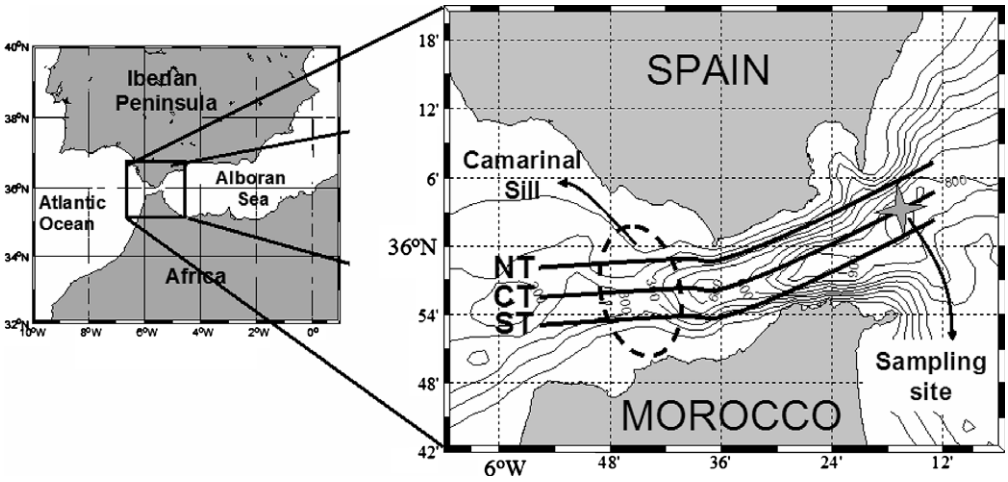

Fig. 1. Area of study. The cross shows the position of the Eulerian station where the diel cycle was observed for comparison to the model results.

and strong tidal currents can give rise to positive correlations between nutrient concentration and tidal flows, in which case, the mean flux into the Mediterranean estimated above assuming steady flows needs to be revised.

One possible way to address these issues is to use numerical models. There have been several attempts to simulate the water circulation through the Strait of Gibraltar using hydrodynamic models (e.g., Wang, 1989, 1993; Brandt et al., 1996; Sein et al., 1998). The models have different levels of complexity ranging from the simplest one-dimensional two-layer model to 3D coarse resolution models. Recently, high spatial-resolution models allowing for realistic bottom topography-flow interaction have been developed: both two-dimensional, two-layer types (Izquierdo et al., 2001; Castro et al., 2004) and three-dimensional ones (Sannino et al., 2002, 2004). All of them have some degree of success in simulating the short-scale undulatory phenomena over Camarinal Sill but they are either unable to deal with mixing (two-layer models) or mixing was not specifically addressed in the study (Sannino et al., 2004).

Currently, there are no physical–biological coupled models that explore the effects of the strong advection and mixing processes on biogeochemical exchanges and the behaviour of the pelagic ecosystem in the Strait and adjacent marine regions. A conceptual model of the plankton distribution in the Strait was proposed by Gómez et al. (2000a) and by Echevarria et al. (2002). This relates the quasi-permanent enrichment of phytoplankton biomass in the north-eastern area of the Strait to mixing processes over the Camarinal Sill and the subsequent eastwards advection of the water masses. However, these authors did not carry out numerical calculations in order to test the conceptual model.

The circulation and its variability are known to modify the distribution patterns of biological variables in the Strait (Gómez et al., 2001; Macías et al., 2006) and in its neighbouring areas (Mercado et al., 2007). Therefore, the correct simulation of the pelagic community in this area must be achieved by means of a physical–biological coupled model in which the physical part can resolve short time-scale dynamic features such as tidal mixing. Physical–biological modelling is actually a fruitful approach promoted by international programs as GLOBEC.

A 2-layer 1-D model is constructed by extracting an along-strait W–E section from the advanced hydrodynamic model of Izquierdo et al. (2001). This 1D model is then modified to improve the representation of vertical tidal mixing. Finally a pelagic biological model is coupled to the physical model. The combined model is used to examine the mixing induced by the tidal circulation (by estimating interfacial shear effects) and its influence on the distribution patterns of biogeochemical fields in the region. The model is described in Section 2, with Section 3 containing our results and Section 4 our conclusions.

2. Models

2.1. Hydrodynamic model

The physical part of the physical–biological model is a 2D, nonlinear, two-layer, free-surface, hydrostatic model with boundary-fitted curvilinear coordinates. Sea-water density is uniform and prescribed in each layer. A complete model description, including governing equations and parameter values used can be found in Izquierdo et al. (2001).

The model is forced at the open boundaries with radiation-type boundary conditions ensuring that when short-wavelength disturbances in the fields of variables are generated they all propagate away from the region of interest. At the coastal boundaries a condition of null normal flow is applied. In order to reduce the influence of any inaccuracies in boundary forcing upon the sought-for solution the waves produced within the strait are allowed to propagate freely through its open boundaries. The staggered Arakawa-C curvilinear grid has a default resolution of 1.0 km decreasing to 0.125 km in the Strait of Gibraltar, with a total of 198×40 gridcells.

The M_2, S_2, K_1 and O_1 surface tidal elevation amplitudes and phases used to set the tidal forcing at the open boundary grid points were derived by interpolating the relevant values from a 0.5° gridded version of the FES95.2 global tidal solutions of Le Provost et al. (1998). The initial mean interface depth was taken from the solution to the 2D steady, two-layer exchange flow problem in the Gulf of Cadiz–Strait of Gibraltar–Alboran Sea system given in Sein et al. (1998). The bathymetry was obtained from the ETOPO5 database complemented by the data from the comprehensive chart published by Instituto Geográfico Nacional and SECEG (1988).

The numerical solution was found by employing an alternating-direction technique with a first-order upstream scheme in the horizontal and a semi-implicit Crank–Nicolson scheme in time. Restricted by the Courant–Friedrichs–Lewy condition the timestep was given a value of 2 s. This time step was used in calculating both the surface and internal tidal modes to avoid averaging of their associated solutions, as would be the case if a time-splitting technique were utilized.

The model was run for 30 identical semidiurnal tidal cycles to achieve a stable time-periodic solution. After establishing this solution, the model run was continued for a 13-month period. The model outputs have been compared to observations in order to assess the validity of assumptions and accuracy of the predictions. After validating the model three along-strait transects at different latitudes have been selected from the two-dimensional grid in order to diagnose mixing and its effects on a biological model. The transects denoted North (NT), Central (CT) and South (ST) (Fig. 1) each consist of 69 grid points separated by 900 m. At each of these points, the hydrodynamic model gives the upper and lower layer along-strait velocity and the interface depth every 15 min for all 13 months of simulation.

2.2. Mixing-advection model

The physical processes influence the biogeochemistry of the region through mixing and advection. Advection velocities for all tracers (see Table 2) are provided directly by the model output. Mixing, which is responsible for variations of concentration, is not directly computed from the hydrodynamic model which is immiscible and therefore does not allow for any exchange of properties between the layers. However, taking into account that interfacial mixing is strongly dependent on the vertical velocity shear across the interface (Briscoe, 1984), we will develop a parameterisation scheme to estimate interfacial mixing. The success of this parameterisation is supported by the reliability of the tidal current predictions of the hydrodynamic model used (Brandt et al., 1996).

Initially, two mixing regimes are identified and parameterised separately. The first is associated with processes that occur at the main sill of Camarinal, where turbulent mixing is strongly enhanced both by the formation of internal hydraulic jumps (Armi and Farmer, 1985) and by arrested internal waves (Bruno et al., 2002). These phenomena produce rates of energy dissipation (and hence, of mixing) that are orders of magnitude greater than the ocean average (Wesson and Gregg, 1994). The second regime parameterises mixing far from the Camarinal Sill and involves the more usual processes of small-scale effectively diffusive mixing.

In our implementation scheme, interfacial mixing is assumed to occur by overturning of the interface in response to the development of Kelvin–Helmhotz (K–H) type instabilities, whose existence is subject to the inequality (Kundu, 1990)

$$g(\rho_2^2 - \rho_1^2) < K\rho_1\rho_2(u_1(t) - u_2(t))^2, \tag{1}$$

being met where K is the wave number of the interfacial disturbances generated by the velocity shear, g is the acceleration due to gravity, ρ_1 and ρ_2 are the fluid densities of the upper and lower layers, and u_1 and u_2 are the velocities in the respective layers. If this criterion is fulfilled, then mixing takes place at the given location in the model.

The amount of material that enters the upper layer from the lower layer after the interfacial overturning may be then estimated by quantifying the change of kinetic and potential energies caused by the overturning, as explained in the following paragraphs and illustrated in Fig. 2.

We will assume that after an interfacial mixing event, a mixing layer of thickness δ_m is eventually formed (see Fig. 2). Taking the vertical co-ordinate as positive upward with zero at the base of the mixing layer, the depth-integrated kinetic and potential energy per unit volume before the overturning event, may be written, respectively, as

$$E_{ki} = \frac{1}{2}\int_0^{\delta_m} \rho(z)u^2(z)\mathrm{d}z = \left[\frac{\rho_1 u_1^2 + \rho_2 u_2^2}{4}\right]\delta_m, \tag{2a}$$

$$E_{pi} = \int_0^{\delta_m} g\rho(z)z\,\mathrm{d}z = \left[\frac{3\rho_1 + \rho_2}{8}\right]g\delta_m^2. \tag{2b}$$

The depth-integrated energies across the mixing layer after the overturning event, may be written as

$$E_{kf} = \delta_m\rho_1(3u_1^2 + 2u_1u_2 + u_2^2)/24 + \delta_m\rho_2(u_1^2 + 2u_1u_2 + 3u_2^2)/24, \tag{3a}$$

$$E_{pf} = g\delta_m^2(2\rho_1 + \rho_2)/6, \tag{3b}$$

where for the sake of simplicity it has been assumed that velocity and density vary linearly across the mixing layer such that

$$u(z) = u_2 + \frac{(u_1 - u_2)}{\delta_m}z,$$

$$\rho(z) = \rho_2 + \frac{(\rho_1 - \rho_2)}{\delta_m}z.$$

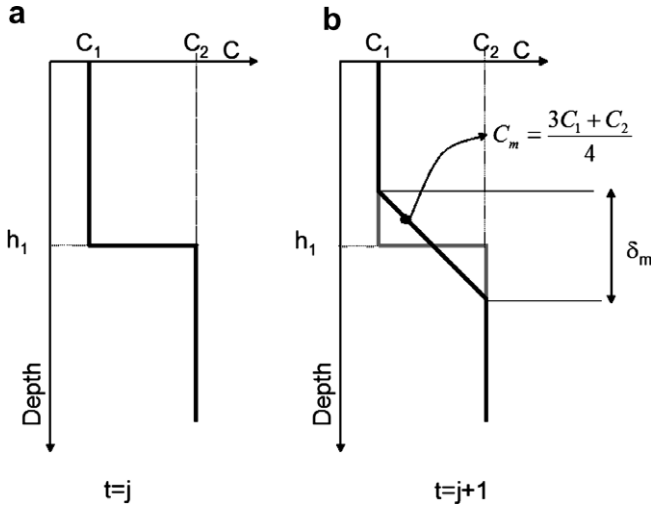

Fig. 2. Schemes of interfacial mixing. (a) Situation before mixing, two layers with homogeneous concentration of a given tracer (C_1 and C_2). (b) After mixing, an interfacial layer is created (thickness δ_m) where concentration varies linearly.

Taking into account that the mixing processes produced by K–H instabilities lead to a conversion of kinetic energy of the sheared flow into potential energy, the changes in potential and kinetic energies, $\Delta E_p = E_{pf} - E_{pi}$ and $\Delta E_k = E_{kf} - E_{ki}$, due to the mixing event, may be related with each other in the following manner:

$$\Delta E_p = -\varepsilon \Delta E_k, \tag{4}$$

where ε is the mixing efficiency, i.e., the proportion of the available kinetic energy transformed into potential energy (De Silva et al., 1999; Peltier and Caulfield, 2003). Using the definitions of Eqs. (2) and (3) to compute the energies before and after the mixing and substituting into Eq. (4), the following relationship between δ_m and ε is obtained:

$$\delta_m = \frac{\varepsilon[\rho_1(3u_1^2 - 2u_1u_2 - u_2^2) - \rho_2(u_1^2 + 2u_1u_2 - 3u_1^2)]}{g(\rho_2 - \rho_1)}. \tag{5}$$

Now, in order to determine the amount of material that is exchanged between the two layers, we will assume that the concentration of a given substance after the interfacial mixing event, follows, as in the case of velocity and density, a linear variation with depth across the mixing layer

$$C(z) = C_2 + \frac{(C_1 - C_2)}{\delta_m} z, \tag{6}$$

where C_1 and C_2 are the concentrations in the upper and lower layer, respectively. Next, we will assume that immediately after the creation of the mixing layer, the upper half of it evolves into a layer of uniform (with depth) concentration. This uniform value is assumed to be the averaged concentration for the upper half of the mixing layer, which may be calculated using Eq. (6) as

$$C_m = C\left(z = \frac{3}{4}\delta_m\right) = \frac{3C_1 + C_2}{4}. \tag{7}$$

Taking into account the amount of material per unit horizontal area contained in the upper half of the mixing layer,

$$M_m = C_m \frac{\delta_m}{2} = \frac{\delta_m}{2} \frac{C_2 - C_1}{4}.$$

If this excess of mass is now assumed to be homogeneously distributed throughout the layer in order to recover the two-layer scheme, the new concentration in layer 1 has increased by $\Delta C_1 = M_m/h_1$. Similar considerations stand for concentrations in layer 2. The time rate at which layer 1 is changing its concentration due to this vertical exchange would be

$$\left(\frac{\Delta C}{\Delta t}\right)_m^{i,j} = \frac{C^{i,j} - C^{i,j-1}}{\Delta t} = \frac{(C_2^{i,j-1} - C_1^{i,j-1})\delta_m^{i,j}}{8h_1^{i,j}\Delta t}, \tag{8}$$

where the superscripts j indicate time (previous $(j-1)$ and current j) and positions (i) where changes are evaluated.

This is the way through which the contribution of the mixing events to the local variation of concentration in the upper layer will be specified. This represents a source/sink term for the given substance. In this way, the mixing-advection equation for an inert tracer in the upper layer could be written as

$$\frac{\partial C}{\partial t} = -\frac{\partial(u_1 C)}{\partial x} + \left(\frac{\partial C}{\partial t}\right)_m, \tag{9}$$

where local changes in concentration result from the net balance between the supplying of substance to the upper layer by interfacial mixing and the advective transport.

Changes of concentration due to interfacial mixing given by Eq. (8), are evaluated each discrete time interval Δt. Therefore, such changes must be understood as an average result from the interfacial mixing processes due to interface overturning events occurring during that time interval and not as an instantaneous change due to a particular overturning event. In this sense, the mixing efficiency, ε, appearing in Eq. (5) must be understood as a bulk parameter characterising the global mixing phenomena occurring during this time interval.

This bulk character must as well be attributed to the mixing layer thickness δ_m. In this way, the mixing model will be dependent on two parameters: mixing efficiency ε and the wave-number K of the K–H instabilities. These parameters are determined by fitting the model output to observations as shown below in this section.

In order to carry out numerical integration of Eq. (9) it will be discretised following the upstream scheme:

$$C^{i,j} = C^{i,j-1} - \frac{\Delta t}{(\Delta x)} u_1^{i,j-1} \Delta C^{j-1} + \frac{(C_m^{i,j} - C^{i,j-1})\delta_m^{i,j}}{2h_1^{i,j}}, \tag{10}$$

with $\Delta C^{j-1} = (C^{i,j-1} - C^{i-1,j-1})$ for $u_1^{i,j-1} > 0$ and $\Delta C^{j-1} = (C^{i+1,j-1} - C^{i,j-1})$ for $u_1^{i,j-1} < 0$. Here, time and spatial (along-strait) coordinates are discretised as $t = j\Delta t$ ($j = 0, 1, 2, \ldots, N$) and $x = i\Delta x$ ($i = 0, 1, 2, \ldots, L$), respectively. The time step of the hydrodynamical model is Δt and Δx is the length of the different cells of the along-strait transect, and the location given by subscripts i are assigned to the centre of the spatial cells. The specific values chosen are $\Delta t = 15$ min and $\Delta x = 900$ m. Before computation of the changes to concentration at the instant (j), the concentration field at instant ($j - 1$) was corrected for numerical diffusion using a 4 iteration MPDATA method (Smolarkiewicz and Margolin (1998)).

Far from the Camarinal area, the term giving the contribution to the upper layer concentration due to the interfacial mixing in Eq. (10) is replaced, prior proceeding to numerical solving by

$$C_m^{i,j} = k_{mix}\left(C_2^{i,j-1} - C_1^{i,j-1}\right), \tag{11}$$

where C_2 is concentration in the lower layer and k_{mix} is an empirical coefficient chosen to best fit the field data. Thus, the change of concentration is assumed to derive from effectively diffusive mixing through the interface. However, the implementation of the semi-empirical three-layer model explained in Section 2.2.2, allows for the use of Eq. (8) for the whole area rather than just over the sill, so that Eq. (11) has only been applied in the two layer scheme explained next.

2.2.1. Mixing in the two layer model

For the two layer model, Eqs. (8) and (11) are used to parameterise mixing depending on the specific area. All the parameters and physical variables involved in those equations are provided by the output of the 2D physical model or prescribed as initial and/or boundary conditions except for parameters δ_m and k_{mix}. The value of δ_m is computed according to Eq. (5) while k_{mix} has been adjusted in order to match the observations of salinity as recorded by the hourly time series collected at the sampling position shown in Fig. 1. The diel cycle was recorded at this location for 25 consecutive hours in November 2003 (Macías et al., 2006).

In Fig. 3, the black line shows the output of the model along CT at the grid point nearest to the sampling station when taking $k_{mix} = 0.5$, which provides the best fit to the observations (dots in Fig. 3). Although some features of the observations like the two peaks of salinity around HW − 4 (the convention HW − n/HW + n indicates n hours before/after high water in Tarifa hereinafter) are acceptably simulated by the model, the shape of the time evolution of observed and modelled data are noticeably different and poorly correlated

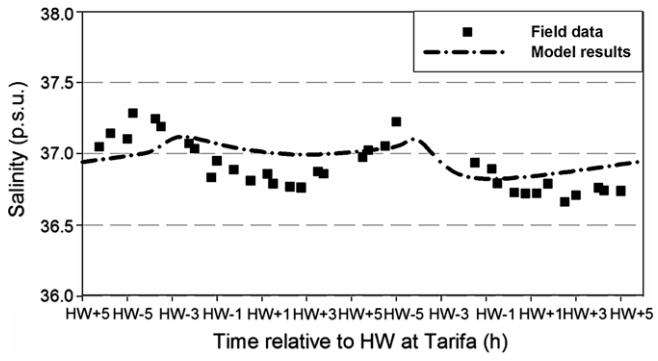

Fig. 3. Measured (squares) and modeled (dot-dashed-line) upper layer salinity along 24 h at the Eulerian station using the two layer model. Horizontal axis is time referred to the High Water (HW) at Tarifa.

($r^2 = 0.3$; $p < 0.01$). Additional runs along NT and ST were carried out but no significant improvement was found.

The differences between the model output and the observations suggest that a two-layer model is too simple to simulate the real system properly. Some studies indicate that a three layer model, the third layer being an interfacial region, is much more appropriate for characterizing the exchange through the Strait of Gibraltar (Bray et al., 1995; Wesson and Gregg, 1994). This more sophisticated approach is addressed in the next section.

2.2.2. Mixing in the three-layer model

The inclusion of a dynamical interfacial region between the upper and lower layers significantly improves the comparison to observations within the Strait. Actually, Bray et al. (1995) estimated that almost 50% of the water transport through the Strait takes place within an intermediate layer. The interfacial layer changes its depth and thickness along the Strait (Bray et al., 1995; Sannino et al., 2002; García-Lafuente et al., 2002) and acts as a buffer for the exchange of properties between the upper and the lower layer. Therefore, the inclusion of this layer provides a more realistic physical scenario for mixing.

With the inclusion of the intermediate layer, there are two interfaces in which mixing must be evaluated: the interface separating the lower and intermediate layer and the interface between the intermediate and upper layer. Obviously the calculation of the thickness of the mixing layer due to K–H instabilities, δ_m, must be evaluated according to Eq. (5) for each one of the two interfaces.

The procedure adopted to determine the intermediate layer thickness is as follows. The step-like velocity profile given by the hydrodynamic model (Fig. 4a) has been transformed into a sigmoidal one (Fig. 13b) as given by the equations:

$$u(z,t) = u_1^t(t) + \frac{a(t)}{1 + e^{-\frac{4}{h_3(t)}[z - z_0(t)]}}, \tag{12.a}$$

with

$$a(t) = \left[\frac{u_2^t(t) - u_1^t(t)}{b_2(t) - b_1(t)}\right], \tag{12.b}$$

$$b_1(t) = \frac{1}{1 + e^{4z_0/h_3(t)}}, \tag{12.c}$$

$$b_2(t) = \frac{1}{1 + e^{-\frac{4}{h_3(t)}[H - z_0(t)]}}, \tag{12.d}$$

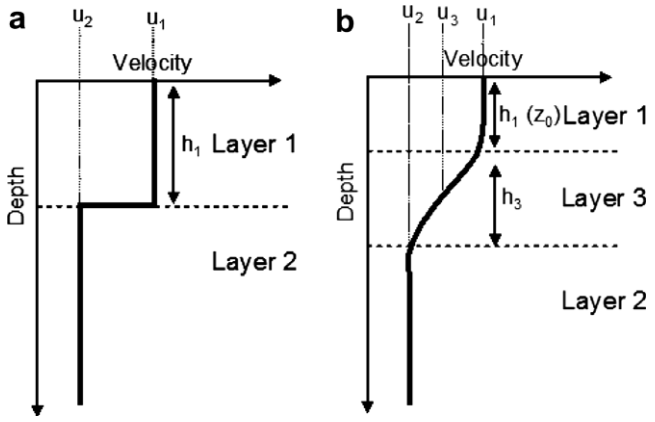

Fig. 4. (a) Original two layer velocity data. (b) Sigmoid-fitting vertical velocity profile. u_1, upper layer velocity; u_2, lower layer velocity; u_3, intermediate layer velocity; h_1, upper layer thickness; h_3, intermediate layer thickness.

where $u_1^t(t)$, $u_2^t(t)$ are the instantaneous velocities in the upper and lower layer far from the influence of the intermediate layer (that is, near the surface and the bottom, respectively). Both velocities are computed under the constraint of keeping the same vertically integrated transport as the two-layer model. H is the bottom depth, $z_0(t)$ is the depth of the centre of the intermediate layer and $h_3(t)$ represents its time-dependent thickness at just one location (Fig. 4b).

The interface thickness is actually a function of time and position, since it fluctuates with tidal periodicity. The time dependence is modelled by including the contribution of the most important tidal constituents of diurnal and semidiurnal species, namely M_2, S_2, K_1 and O_1 which were already included as forcing terms in the physical model. Explicitly, $h_3(t)$, has been assumed to vary according to

$$h_3(t) = \overline{h_3} + \sum_{i=1}^{M} A_i U_i \cos(\omega_i t - g_i - \Delta g_i), \tag{13}$$

where $\overline{h_3}$ is the time-averaged interface thickness, U_i and g_i are the harmonic constants (amplitude and Greenwich phase) of the 'i'th component of the lower layer velocity, ω_i is its frequency, M is the number of component frequencies used in the harmonic expansion (4 in our case) and A_i and Δg_i are the gain and phase lag, respectively, of the transfer function between lower layer velocity (input) and interface thickness (output) obtained from a correlation analysis, in the frequency domain, of velocity time series in the main sill of Camarinal recorded by an ADCP moored during years 1994 and 1996. Using ADCP data the region of maximum velocity shear was used to estimate the thickness of the interface. Fig. 5 shows the good agreement between the estimated and the predicted thickness using Eq. (13). The observed changes of more than 120 m in interface thickness (40% of the total water depth in Camarinal) demonstrate why it is important to have reliable estimates of the interface thickness if it is intended to reproduce tidal mixing in the Strait.

The time-averaged thickness of the interface, $\overline{h_3}$, has been taken from the work of Sannino et al. (2002). Therefore, the sigmoidal profile $u(z,t)$ may be fully determined and it replaces the step-like profile of the two-layer model in all computations involving advection and mixing of properties. Eq. (13) can be used to characterise the interface thickness along the entire longitudinal axis of the Strait, while Eq. (12) defines the vertical profile of velocities throughout the area. Thus it is possible to calculate the thickness of the intermediate mixing layer using Eq. (13) at all points on the along-strait transect.

The improvement of the three layer approach relative to the two-layer model is illustrated by Fig. 6. The black thick line represents the new prediction of salinity at the position of the sampling station. The model reproduces the periodicity and the amplitude of the salinity peaks (though slightly overestimates the maxima) once again. Furthermore, the shape of the modelled salinity is much more similar to the observations (correlation coefficient $r^2 = 0.84$; $p < 0.01$). This prediction, which yielded the best fit to the observations, was achieved for a value of mixing efficiency $\varepsilon = 0.10$ along with a value of K–H instabilities wave-number $K = 4.18 \times 10^{-2}\ \mathrm{m}^{-1}$ (wave-length of 150 m), values that are in good agreement with other reported experimental values (Osborne, 1980; Peltier and Caulfield, 2003).

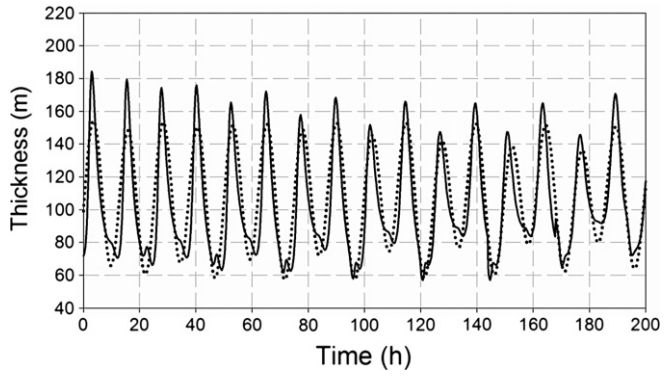

Fig. 5. Observed (solid line) and predicted (dotted line) thickness of the interface (m) over the Camarinal Sill during 9 days of simulation.

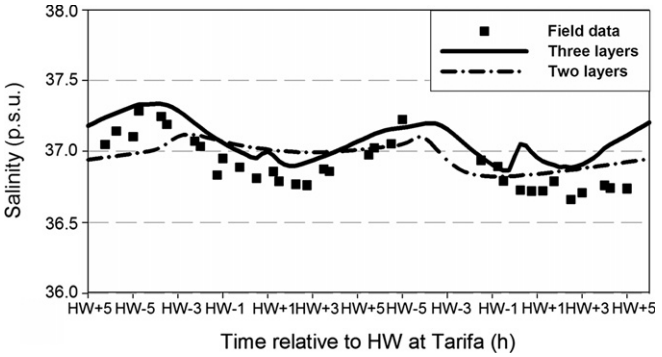

Fig. 6. Measured (squares) and modeled upper layer salinity at the Eulerian station during 24 h. Two (dot-dashed-line) and three (solid line) layer models.

Therefore, the incorporation of an intermediate layer is seen to significantly improve the performance of the mixing model. The differences between the model output and the observations that are seen in Fig. 6 may be due to horizontal cross-strait advection, which is not taken into account in our model. Further evidence for this is discussed later.

Interfacial mixing in the three-layer model includes mixing between the lower and the interface layers as well as mixing between the interface and the upper layers. Each of these processes can be estimated from Eq. (8) by using the two values of δ_m calculated according to Eq. (5). As mentioned above, interfacial mixing is now allowed for along the whole Strait. With this new formulation, the changes of interface layer thickness modulate the intensity of the mixing, which is illustrated in Fig. 7 for several days. Not surprisingly, there is intense and pulsating mixing over the Camarinal Sill although the most intense interfacial mixing occurs eastwards of Tarifa Narrows (see label in the bottom panel of Fig. 7). This happens because in this part of the Strait the interface tends to be shallower (Bray et al., 1995) and thicker (García-Lafuente et al., 2002) than elsewhere. The upper layer becomes thinner gradually and, thereby, its velocity increases to satisfy mass conservation. Therefore, the velocity shear is enhanced in this region and the interfacial mixing increases. A similar result was suggested by Sannino et al. (2004) when analysing water entrainment/detrainment forced by tides. As expected, two mixing-enhanced events happen every day, indicating the tidally-related periodicity of the phenomenon. They correspond to the increased shear that takes place during flood tide (García-Lafuente et al., 2000; Izquierdo et al., 2001; García-Lafuente et al., 2002). However, there is some uncertainty in the estimates of the amount of interchange between layers driven by vertical mixing processes in the Strait of Gibraltar based on field measurements (Minas and Minas, 1993), due to the high variability of the physical environment.

2.3. Biogeochemical model

The biological model is a simple nitrogen-based Nutrient–Phytoplankton–Zooplankton (NPZ) model. Its structure and constituent processes are depicted in the diagram of Fig. 8. To agree with the numerical grid of the hydrodynamical model for the along-strait transects, the upper layer have been divided into fixed volume cells with the same along-strait length. The temporal changes in concentration of the constituents we are interested on, within each one of these cells, are given by the equations

$$\frac{\partial N}{\partial t} = -\frac{\partial (u_1 N)}{\partial x} + \left(\frac{\partial N}{\partial t}\right)_m + (1-\beta) G_p + \Omega \frac{m_z Z^2}{k_z + Z} - JQ\mu_p P, \tag{14}$$

$$\frac{\partial P}{\partial t} = -\frac{\partial (u_1 P)}{\partial x} + \left(\frac{\partial P}{\partial t}\right)_m + JQ\mu_p P - G_p - m_p P, \tag{15}$$

$$\frac{\partial Z}{\partial t} = -\frac{\partial (u_1 Z)}{\partial x} + \left(\frac{\partial Z}{\partial t}\right)_m + \beta G_p - \frac{m_z Z^2}{k_z + Z}, \tag{16}$$

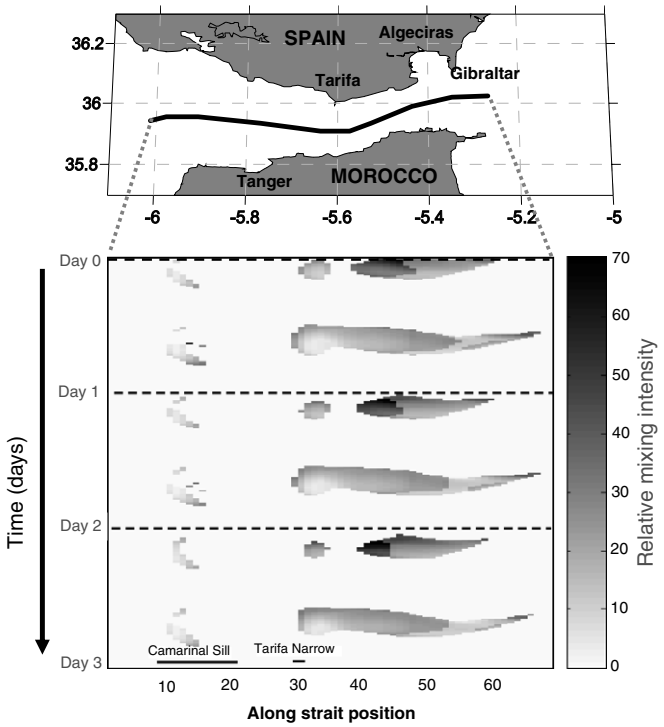

Fig. 7. Mixing intensity between upper and intermediate layers during three days of simulations calculated according to Eq. (10).

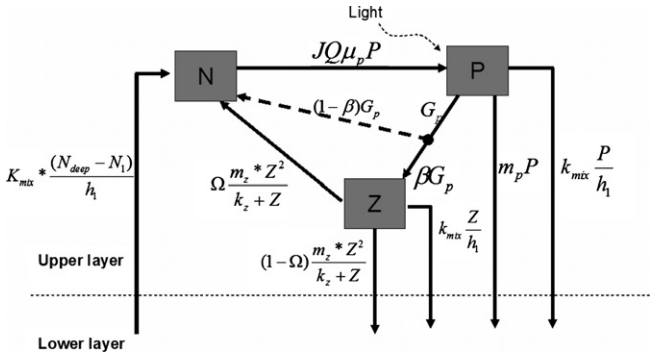

Fig. 8. Conceptual diagram and equations of the NPZ model used. The arrows entering the lower layer in the diagram indicate losses from the modelled system.

where

$$Q = \frac{N}{k_1 + N}, \tag{17}$$

$$G_{\mathrm{p}} = \frac{gP^n}{k_g^n + P^n} Z, \tag{18}$$

and J expresses light limitation of phytoplankton growth *sensu* Evans and Parslow (1985).

The term $(\partial C/\partial t)_{\mathrm{m}}$, represents the local temporal rate of change in concentrations due to the interfacial mixing, as has been explained in Section 2.2. The term $\partial(u_1 C)/\partial x$ represents changes in concentration due to the advective horizontal transport of the water mass in the upper layer. The rest of the variables and parameters are explained in Fig. 8 and Table 1.

Table 1
Model parameter symbol, description, values and used source

Symbol	Parameter	Value	Source
μ_p	Phytoplankton maximum growing rate (d^{-1})	3.0	Eppley et al. (1969)
λ	PAR fraction of solar radiation	0.43	Fasham et al. (1993)
k_w	Attenuation coefficient of water, m^{-1}	0.04	Fasham et al. (1993)
α	Initial slope of *P–I* curve $(W m^{-2})^{-1} d^{-1}$	0.104	Fasham (1995)
k_1	Half saturation for nitrate uptake (mmol m^{-3})	0.5	Fasham et al. (1993)
N_{deep}	Nitrate concentration in lower layer (mmol m^{-3})	9.8	Field data
m_p	Phytoplankton maximum natural mortality rate (d^{-1})	0.05	Fasham et al. (1993)
k_c	Self-shading coefficient, m^{-1} $(mmol\ m^{-3})^{-1}$	0.03	Fasham et al. (1993)
g	Maximum zooplankton grazing rate (d^{-1})	1	Fasham et al. (1993)
β	Zooplankton ingestion efficiency	0.75	Fasham et al. (1993)
a	Air-sea albedo	0.05	Fasham et al. (1993)
k_{mix}	Cross picnocline mixing (m d^{-1})	0.5	
k_g	Zooplankton ingestion half saturation (mmol m^{-3})	1.0	Fasham et al. (1993)
Ω	Fraction of zooplankton loss term to nutrient	0.25	Fasham et al. (1993)
m_z	Zooplankton maximum mortality rate, d^{-1} $(mmol\ m^{-3})^{-1}$	0.325	Fasham et al. (1993)
k_z	Half-saturation of zooplankton mortality (mmol m^{-3})	0.2	Fasham et al. (1993)

Table 2
Model boundary and initial conditions for upper and lower layer

	Upper layer (mmol N/m^{-3})	Lower layer (mmol N/m^{-3})
Nitrate	1.2	9.8
Phytoplankton	0.21	0.0032
Zooplankton	0.05	0
Salinity	36.5 (p.s.u.)	38 (p.s.u.)

Boundary and initial conditions for the concentration of nutrients, phytoplankton and zooplankton are presented in Table 2. The values come from the analysis of more than 150 field data taken all over the Strait at five different depths during four different cruises carried out in different years. They are in good agreement with previous observations in the region (Gómez et al., 2000b; Minas et al., 1991; Dafner et al., 2003).

The phytoplankton and zooplankton that fall through the interface enter the lower layer and are no longer considered by the model (as the concentration in the lower layer is constant for all the state variables). At the eastern boundary of the model there is a zero gradient boundary condition for surface concentrations as the flow is always eastward and hence out of the model. In the upper layer at the western boundary concentrations are fixed to constant values (showed in Table 2) as the flow can reverse over a tidal cycle. Although direct observations are used to constrain the constants used for the western boundary conditions, there may remain concerns over the fact that they are not allowed to vary with time. For this reason, sensitivity analyses are done, as discussed later.

The physical part of the model influences the biological component by advecting the biological tracers horizontally and by mixing them vertically between the layers. To avoid the effect of transients, the coupled model was left to evolve for 3 days (300 time steps) before starting the real simulation. It was confirmed that this period of time was enough for transients to die out.

The NPZ model is a very simple description of the pelagic plankton ecosystem. A more complex model, like that described by Fasham et al. (1990, 1993) with seven different compartments including bacteria and detritus, has also been run but the differences in model performance are very small for N, P and Z (Fig. 9 shows differences for phytoplankton only). Therefore, for the sake of simplicity and because "*there is no compelling reason to reject the NPZ until is clear that it cannot describe the system being studied*" (Franks, 2002), the model described by Eqs. (14)–(18) has been used in this paper. Furthermore, it is more straightforward to change parameter values or boundary conditions in the NPZ model.

As mentioned above, the model was run for 13 months, with a time step of 15 min. In each time step the following state variables were calculated at the 69 gridcells in the different layers: salinity (p.s.u.), nitrate

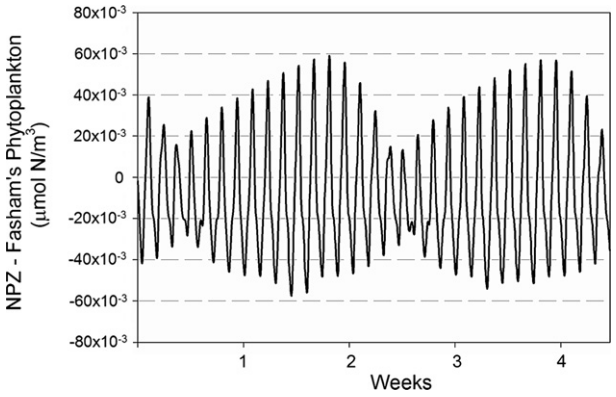

Fig. 9. Differences in mean Phytoplankton concentration in the upper layer using a Fasham's-like and an NPZ formulation, during 4.5 weeks.

(mmol N/m^3), phytoplankton (mmol N/m^3), zooplankton (mmol N/m^3), pseudo-phytoplankton (mmol N/m^3) and an exponentially decaying tracer. Nitrogen is a common currency of marine models (Fennel and Neumann (2004)) as biologically available nitrogen is frequently a limiting nutrient for primary production in the ocean. In the Mediterranean basin phosphate is usually regarded as the limiting nutrient; however we use nitrogen as currency of the model because all the biogeochemical processes are going to happen in the upper (Atlantic) layer. Moreover, our own measurements (data not shown) and those made by Gómez et al. (2000b) clearly indicate that in the surface layer of the Strait of Gibraltar nitrogen is the limiting nutrient as N:P is, usually, well bellow the threshold Redfield value (Redfield et al., 1963).

Pseudo-phytoplankton is an inert tracer with the same initial and boundary values of the phytoplankton but undergoing no biogeochemical reactions. Hence the differences between phytoplankton and the pseudo-phytoplankton are solely the consequence of biological interactions (growth, death or consumption). The decaying tracer suffers exponential decay with a fixed half life. This allows us to determine the time that a water parcel resides within the model domain.

3. Results and discussion

3.1. Nutrient budget

Estimates of nutrient fluxes given in the introduction for the case of no-mixing and steady exchange are not realistic due to the role that mixing plays in the inter-layer exchange of properties. The calibration exercise carried out for salinity demonstrates the necessity to include mixing in any model of the Strait. Having incorporated mixing, the model allows us to estimate the amount of nitrogen in the outflowing layer that is introduced in the upper layer by mixing and thereby recirculated into the Mediterranean Sea.

The concentration of nutrient in the upper layer of the model is a function of the tidal amplitude and the percentage of the outflowing nitrate recirculating back into the Mediterranean due to interfacial mixing is correlated with tidal amplitude ($r^2 = 0.7$; $p < 0.01$). The fraction of nutrient recirculation is also dependent on the state of the tide, varying between 4% and 35% with an average of 16.3%. This value is in good agreement with previous estimates based on field measurements (Table 3), although it is in the lower end of the measured range. One hypothesis for the slightly low value predicted by our model is its 1-D character, which neglects 2-D effects such as the cross-strait advection already mentioned. Flow-topography interactions favour mixing and upwelling processes in the shallower marginal areas to the sides of the modelled transects. These processes, in turn inject nutrients laterally into the upper layer in a manner that our 1-D model is unable to capture. These marginal processes may also influence the chlorophyll distribution as discussed in the next Section. The only source of nutrient to the upper layer in the three-layer scheme is the mixing between the surface Atlantic layer and the deeper Mediterranean waters. The contribution of the relatively nutrient-rich North

Table 3
Estimate of nutrient recirculation by other authors and by the current model

Source	% of nutrient recirculation
Wesson and Gregg (1994)	20
Gómez et al. (2000b)	21
Dafner et al. (2003)	16
This work	16.3 (4–35)

Atlantic Central Water (Packard et al., 1988) is not considered, though it is known that this water could be upwelled during some phases of the tidal cycle, being incorporated into the main along strait circulation (e.g., Gómez et al., 2001; Macías et al., 2006). The lateral injection of nutrients commented on above is also not included and could lead to underestimations. Table 3 however indicates that the likely underestimation is not significant.

The daily mean amount of nutrients introduced into the Mediterranean by the Atlantic inflow computed from our model is shown in Fig. 10 for a period of one year. The dominant variability has a fortnightly period (see details in Fig. 10b), indicating strong tide-related forcing of the recirculation processes. The year-averaged value is 2272.8 mol N/s but it fluctuates between a minimum of around 1200 mol N/s and a maximum greater than 3500 mol N/s. The average value must be compared with the mean amount of nutrients advected into the Mediterranean Sea in the case of no-mixing, steady exchange as discussed in the introduction. The value of 972 mol N/s computed for that case increases to 2272.8 mol N/s if interfacial mixing is taken into account,

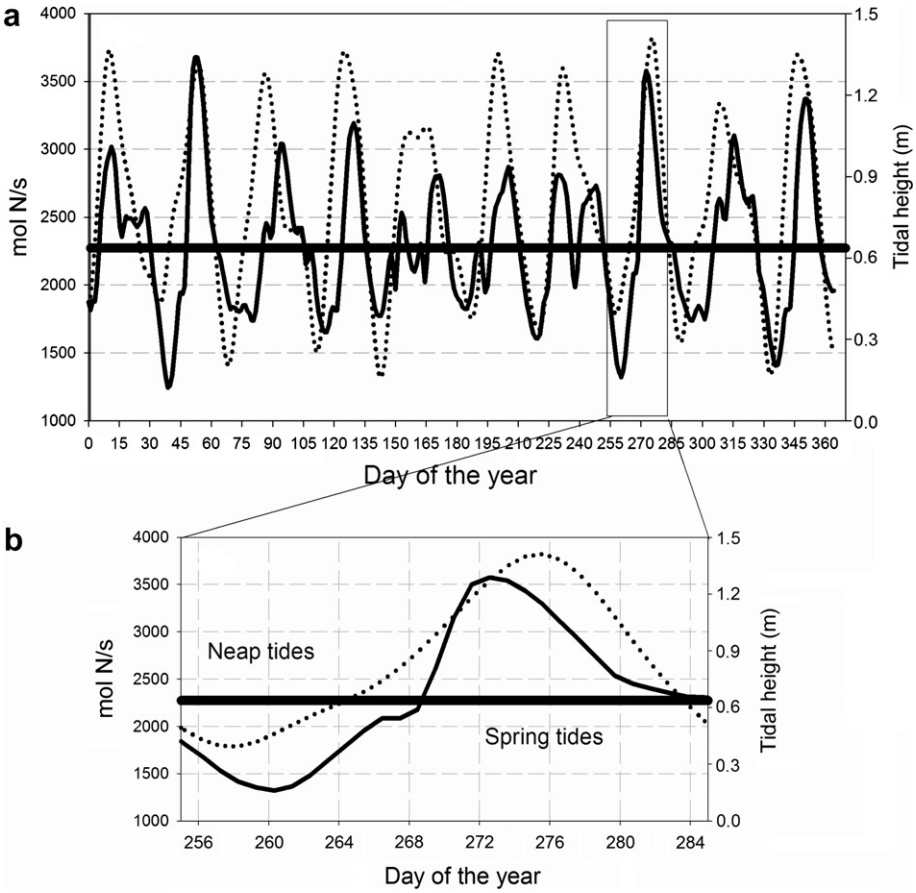

Fig. 10. Mean daily flux of nutrient in the upper layer towards the Mediterranean (thin solid line) and tidal height (dotted line). (a) During the whole simulation. (b) During 30 days. Thick solid line indicates the mean carbon nitrogen flux over all the period.

that is, an increase of 130%. Obviously, mixing driven by tides cannot be neglected when computing nutrient fluxes. A consequence of this is that the estimates made with field data collected over a limited period of the year will differ from the real annual mean values by a factor depending on the amplitude of the tide during the sampling period.

3.2. Plankton dynamics

One of the most interesting effects of the tidally-induced mixing from a biological point of view is the fertilisation of illuminated surface waters. Tidally-induced mixing in the Strait supplies nutrients to the phytoplankton in the photic layer, which might be thought to result in a positive relation between tidal amplitude and phytoplankton abundance. However, a negative correlation ($r^2 = 0.2$; $p < 0.01$) between tidal amplitude and phytoplankton concentration in the upper layer is found, indicating that the phytoplankton is unable to utilise fully the amount of nutrient available through mixing.

An explanation for this behaviour is provided by the model simulations, which show that interfacial mixing produces strong dilution of the phytoplankton in the upper layer because of the low concentration of cells in the lower layer (see Table 2). As a result, the annual average concentration of phytoplankton in the upper layer decreases from west to east (Fig. 11a).

Modelled phytoplankton and pseudo-phytoplankton concentrations show largest differences in the eastern side of the Strait (Fig. 11b). Taking into account that both concentrations are identical in the western part of the domain and that pseudo-phytoplankton is an inert tracer whereas phytoplankton undergoes biological processes, the obvious explanation for the different concentrations in the eastern side is that phytoplankton experience a net population growth while they are advected through the Strait. The population growth is not large enough, however, to compensate losses due to mixing-related dilution and therefore the net concentration of phytoplankton in the upper layer decreases towards the east.

The increase in phytoplankton concentration in the model passing through the channel is low (maximum of 0.05 mmol N/m^3), because of the short residence time of cells within the model domain. An average phytoplankton cell only takes 25 h to cross the Strait from west to east in the upper layer (Fig. 12). The maximum growth rate of the phytoplankton is 3.0 d^{-1} (Table 1) and, considering the small initial concentrations of phytoplankton (Table 2), there is no time for sufficient growth of the population regardless of the amount of nutri-

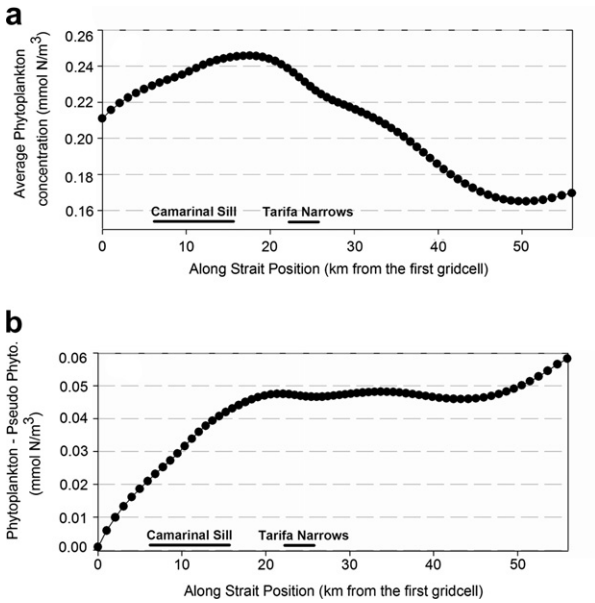

Fig. 11. (a) Average concentration of Phytoplankton in the upper layer for each position of the section throughout 13 month of simulation. (b) Differences between phytoplankton and pseudo-phytoplankton at each position for the same period.

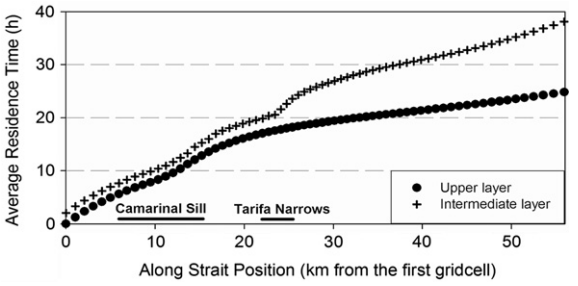

Fig. 12. Average residence time of the water at each position in the upper and intermediate layer for all the simulation.

ents available. Sensitivity analyses have been conducted increasing the western boundary concentration of phytoplankton by up to a factor of 10 times the standard value but there is no significant change in the results obtained, the decrease of the phytoplankton concentration in the eastern side of the Strait being a robust feature. The strong advection is the limiting factor and the coupled physical–biological model is dominated by hydrodynamic-controlled patterns, suggesting why more complex biological models are not necessary (Section 2.3). The short transit time due to the strong advection is especially marked in the upper layer where there is a high velocity, but even in the intermediate layer, where the advection speed is lower, we have calculated residence times that barely reach 38 h, indicating an annual average speed of 0.4 m/s (Fig. 12).

In contrast to these model results, some field observations show high chlorophyll concentration in the eastern side of the Strait (Minas et al., 1991; Gómez et al., 2001; Echevarria et al., 2002). Local growth of phytoplankton populations while crossing the Strait in an environment enriched by the mixing-driven injection of nutrients in Camarinal Sill has previously been put forward to explain these observations (Reul et al., 2002) Other works (Packard et al., 1988; Ruiz et al., 2001) propose that noticeable increase of phytoplankton concentrations in the Atlantic layer away from the Strait can be better explained by the influence of mixing in the Strait than by local enrichment in the Alboran basin, due to the usual large advection velocities of the Atlantic jet that would imply the observation of these effects in the north-western Alborán Sea or, even, much further west, in the Almería-Orán front, at the east of the Alborán Sea (Arnone et al., 1990). These latter results would agree with the predictions of the model, which indicates a residence time in the main channel too short to allow for a significant growth of phytoplankton during its transit through the Strait, even if the cells reside in the intermediate layer (Fig. 12).

Another characteristic feature observed in the area is the chlorophyll enrichment of the north-eastern side of the channel compared with the southern section (Gómez et al., 2000a). From the perspective of Sverdrup's critical-depth theory this differential behaviour could be related to a combination of the lower advection velocity of the inflowing waters in the north together with the shallower interface (Gómez et al., 2000a; Reul et al., 2002). The model runs for the NT still give an averaged residence time in this transect of around 26 h, which is only 1 h more than in the central or the southern section. Therefore, the increase in the residence time in the NT is not the correct explanation for the observed patterns.

In order to assess the model predictions, the modelled phytoplankton concentration in the upper layer has been compared with the observations collected during the diel cycle carried out at one site in the eastern end of the Strait (see Fig. 1 for position). Fig. 13 shows that observations exhibit two peaks of high concentration around HW-4 simultaneous to the peaks of salinity shown in Fig. 6, although the distribution of phytoplankton has higher dispersion than that of salinity. The peaks are twelve hours apart, indicating tidal periodicity in the forcing of the phytoplankton peaks. Although the model output shows similar behaviour, it has two important drawbacks. First, it must be noticed that scales for modelled (left) and observed (right) concentrations in Fig. 13 are different, so the observed concentration of phytoplankton is about twice larger than the concentration predicted by the model. Second, there is also a clear difference in the time when predicted and observed maxima appear, the maximum observed concentration coinciding with a minimum of predicted abundance and vice versa (correlation coefficient $r^2 = 0.3$, $p < 0.01$). Although the model predicts the spatial distribution of salinity reasonably well, is not able to predict phytoplankton abundance satisfactorily, a fact that stands independently of the complexity of the biogeochemical model.

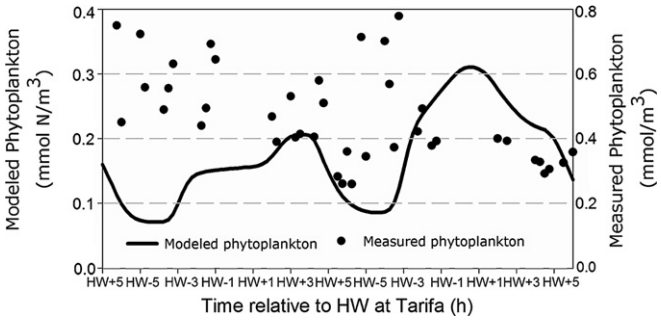

Fig. 13. Measured and modeled Phytoplankton concentration (mmol N/m^3) in the upper layer along 24 h. at the Eulerian station.

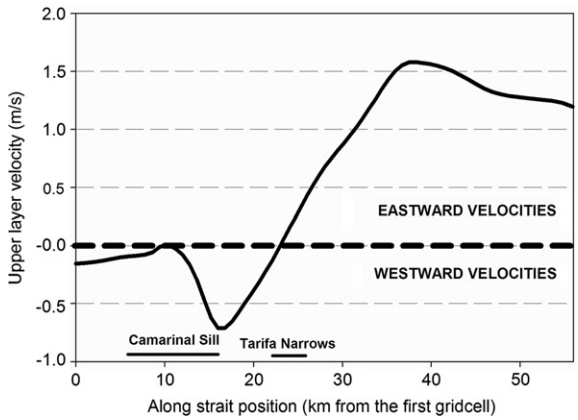

Fig. 14. Upper layer velocity (m/s) along the central section near the High Water time.

With the residence times predicted by the model, it is clear that the high levels of chlorophyll measured in the eastern section of the Strait must be the result of something other than local growth. Another source of chlorophyll is necessary in order to explain the high concentration observed in the eastern section. In the western part of the Strait, the currents in the surface layer reverse during part of the semidiurnal tidal cycle (Béthoux and Copin-Montégut, 1986; Candela, 1990) while they hardly ever reverse east of Tarifa Narrows (García-Lafuente et al., 2000), giving rise to intense divergences in the upper layer. The physical model reproduces this phenomenon and indicates that the divergence takes place between Tarifa Narrows and Camarinal sill around high water (Fig. 14).

Internal oscillations of the interface can partly account for the upper layer divergence (García-Lafuente et al., 2000) but some compensation by horizontal flow from both north and south coastal areas cannot be disregarded. The input from the chlorophyll-rich coastal surface waters into the central channel would increase the chlorophyll concentration periodically by means of a mechanism not specified in our model. Some evidence of suction of coastal waters through the Strait is provided by van Genn et al. (1988), who suggest that the high concentrations of trace metals in the Mediterranean surface waters when compared with open ocean Atlantic waters could be explained by the advection through the Strait of Gibraltar of waters from the continental shelf of the Gulf of Cadiz.

Horizontal advection from the north and south is also supported by the following discussion. If there is no horizontal advection, salinity and phytoplankton concentration must be negatively correlated because salinity increases when interfacial mixing is enhanced but phytoplankton concentration diminishes by dilution. The model predicts this behaviour but observations behave in the opposite manner (Fig. 15). The contradiction can be overcome if coincidentally with intense interfacial mixing there is advection of coastal chlorophyll-rich waters to the interior of the channel. Since interfacial mixing is favoured by the undulatory processes in Cam-

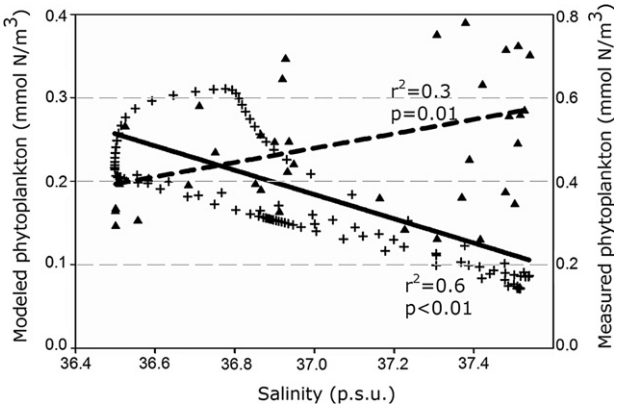

Fig. 15. Measured (triangles, dashed line) and modeled (crosses, solid line) phytoplankton vs. salinity in the Eulerian station.

arinal (Wesson and Gregg, 1994) and divergence usually happens when undulatory processes are active (Izquierdo et al., 2001), it follows that interfacial mixing and divergences are simultaneous and, hence, so would be horizontal advection and intense mixing. An indirect proof for this is the recent result of a series of Longhurst-Hardy Plankton Recorder (LHPR) casts along the Strait crossing over Camarinal sill presented by Echevarria et al. (2005). A first leg carried out at HW-3 registered low concentration of particles but a later leg around HW-1 found great concentration of chlorophyll and plankton biomass over the sill. At this time, dilution should have reduced the chlorophyll concentration due to the strong mixing but it actually showed enhanced levels, thus suggesting horizontal advection from the north and south as one likely mechanism of chlorophyll supply. Notice that horizontal advection has no impact on salinity since coastal and open channel waters have similar values (Navarro, 2004; García-Lafuente and Ruiz, 2007).

The coincidence of the highest concentrations of chlorophyll with the presence of undulations would lead to a packaging of the cell peaks in patches as such undulations are able to create convergence and divergence alternating areas. Pulse trains comprising patches of high chlorophyll travelling eastward within the Atlantic layer was observed by Macías et al. (2006) during several diel cycles performed in the eastern side of the Strait, at different dates in the years 2002 and 2003. Moreover, in that work a clear correlation between the maximum chlorophyll levels and the presence of undulatory disturbances in the Atlantic–Mediterranean interface waters was found.

Other processes, such as suction of coastal waters from other areas (such as the Algeciras Bay) or, even, the advection of chlorophyll patches from the Alboran Sea coastal areas to the east side of the Strait could be involved in the observed patterns. More field sampling and modelling exercises must be done to elucidate the relative importance of those processes.

4. Conclusions

This paper illustrates how a simple 1-D physical–biological coupled model with just three-layers in the vertical is capable of simulating the distribution of salinity in an along strait section, by estimating the interfacial mixing and advection through the main channel of the Strait of Gibraltar.

This model gives a reasonable description of the main interchange processes between the Mediterranean and Atlantic waters in the Strait. Model output shows a large amount of nutrients leaving the deep waters and being injected into the upper layer, with a clear correlation with the fortnightly tidal amplitude variations. The calculations show that these upwelled nutrients must be taken into account if the behaviour of the phytoplankton in the Alborán Sea, adjacent to the Strait, is going to be addressed.

However, the model cannot fully simulate the behaviour of biological tracers such as phytoplankton, as these can be strongly influenced by processes occurring outside the domain of the model (i.e., in horizontally-neighbouring regions). This work also demonstrates that the residence time of water within the Strait is too short to account for the quasi-permanent enrichment of chlorophyll observed in the north-eastern sector

of the Strait. The residence time is also very short in the interfacial layer. Increases in phytoplankton concentrations cannot, therefore, be related simply to phytoplankton growth in the channel axis. It is very likely that the suction (by upper layer divergences) of coastal, chlorophyll-rich water from the margins into the main along strait circulation occurs.

To achieve a better understanding of biological processes in the Strait more complex models should be developed, including 2D (and/or 3D) models to analyse the marginal mixing, channel-shelf exchanges, and lateral mixing in the Atlantic jet entering the Mediterranean. This should of course be backed up with corresponding observations.

Acknowledgments

This work has been funded by the Projects of the Spanish National Research Program REN-2001-2733-C02-01/02 and CTM2005-08142-C03-01/02. Diego Macías and Agueda Vázquez were supported by grants of the Spanish FPI fellowship program. Adrian Martin was funded by an NERC UK Research Fellowship. A. Izquierdo was partially supported by Spanish Project VEM2003-20577-C14-07. JGL acknowledges partial support from Spanish National Research Projects REN2003-01608 and CTM-2006-02326.

References

Armi, L., Farmer, D., 1985. The internal hydraulics of the Strait of Gibraltar and associated sill and narrows. Oceanologica Acta 8 (1), 37–46.

Armi, L., Farmer, D., 1988. The flow of Mediterranean Water through the Strait of Gibraltar. Progress in Oceanography 21, 41–82.

Arnone, R.A., Wiesenburg, D.A., Saunders, K.D., 1990. The origin and characteristics of the Algerian current. Journal of Geophysical Research 95 (C2), 1587–1598.

Basheck, B., Send, U., García Lafuente, J., Candela, J., 2001. Transport estimates in the Strait of Gibraltar with a tidal inverse model. Journal of Geophysical Research 106, 31033–31044.

Béthoux, J.P., Copin-Montégut, G., 1986. Biological fixation of atmospheric nitrogen in the Mediterranean Sea. Limnology and Oceanography 31 (6), 1353–1358.

Béthoux, J.P., Morin, P., Chaumery, C., Connan, O., Gentili, B., Ruiz-Pino, D., 1998. Nutrients in the Mediterranean Sea, mass balance and statistical analysis of concentrations with respect to environmental change. Marine Chemistry 63, 155–169.

Boyce, F.M., 1975. Internal waves in the Strait of Gibraltar. Deep-Sea Research 22, 597–610.

Brandt, P., Alpers, W., Backhaus, J.O., 1996. Study of the generation and propagation of internal waves in the Strait of Gibraltar using a numerical model and synthetic aperture radar images of the European ERS 1 satellite. Journal of Geophysical Research 101 (C6), 14237–14252.

Bray, N.A., Ochoa, J., Kinder, T.H., 1995. The role of interface in exchange through the Strait of Gibraltar. Journal of Geophysical Research 100 (C6), 10755–10776.

Briscoe, M.G., 1984. Tides, solitons and nutrients. Nature 312, 15–18.

Bruno, M., Alonso, J.J., Cózar, A., Vidal, J., Ruiz-Cañavate, A., Echevarría, F., Ruiz, J., 2002. The boiling-water phenomena at Camarinal Sill, the strait of Gibraltar. Deep-Sea Research II 49, 4097–4113.

Bryden, H.L., Kinder, T.H., 1988. Gibraltar experiment: a plan for dynamic and kinematic investigation of strait mixing, exchange and turbulence. Oceanologica Acta N_SP.

Bryden, H.L., Kinder, T.H., 1991. Steady two-layer exchange through the Strait of Gibraltar. Deep Sea Research 38S, S445–S463.

Bryden, H.L., Candela, J., Kinder, T.H., 1994. Exchange through the Strait of Gibraltar. Progress in Oceanography 33, 201–248.

Candela, J., 1990. The barotrophic tide in the Strait of Gibraltar. The Physical Oceanography of Sea Straits. K.A. Publisher, pp. 457–475.

Castro, M.J., García-Rodriguez, J.A., González-Vida, J.M., Macías, J., Parés, C., Vázquez-Cendón, M.E., 2004. Numerical simulation of two-layer shallow water flows through channels with irregular geometry. Journal of Computational Physics 195, 202–235.

Dafner, E.V., Boscolo, R., Bryden, H.L., 2003. The N:Si:P molar ratio in the Strait of Gibraltar. Geophysical Research Letters 30 (10), 13.1–13.4.

De Silva, I.P.D., Brandt, A., Montenegro, L.J., Fernando, H.J.S., 1999. Gradient Richardson number measurements in a stratified shear layer. Dynamics of Atmospheres and Oceans 30, 47–63.

Echevarria, F., García-Lafuente, J., Bruno, M., Gorsky, G., Goutx, M., González, N., García, C.M., Gómez, F., Vargas, J.M., Picheral, M., Striby, L., Varela, M., Alonso, J.J., Reul, A., Cózar, A., Prieto, L., Sarhan, T., Plaza, F., Jiménez-Gómez, F., 2002. Physical–biological coupling in the Strait of Gibraltar. Deep-Sea Research II 49 (19), 4115–4130.

Echevarria, F., Somavilla, R., Bruno, M., González-Gordillo, J.I., Becognee, P., Izquierdo, A., Macías, D., Vázquez, A., García, C.M., 2005. Plankton biomass distribution in the central channel of the Strait of Gibraltar: aggregation as a response to physical forcing. ASLO Summer Meeting, Santiago de Compostela, unpublished.

Eppley, R.W., Rogers, J.N., McCarthy, J.J., 1969. Half saturation constrats for uptake of nitrate and ammonium by marine phytoplankton. Limnology and Oceanography 14, 912–920.

Evans, G.T., Parslow, J.S., 1985. A model of annual plankton cycles. Biological Oceanography 3 (3), 327–347.
Fasham, M.J.R., 1995. Variations in the seasonal cycle of biological production in subarctic oceans: A model sensitivity analysis. Deep-Sea Research 42, 1111–1149.
Fasham, M.J.R., Ducklow, H.W., McKelvie, S.M., 1990. A nitrogen-based model of plankton dynamics in the oceanic mixed layer. Journal of Marine Research 48, 591–639.
Fasham, M.J.R., Sarmiento, J.L., Slater, R.D., Ducklow, H.W., Williams, R., 1993. Ecosystem behaviour at Bermuda Station S and Ocean Weather Station India: a general circulation model and observational analysis. Global Biochemical Cycles 7, 379–415.
Fennel, W., Neumann, T., 2004. Introduction to the modelling of marine systems. Elsevier B.V., Amsterdam.
Franks, P.J.S., 2002. NPZ models of plankton dynamics: their construction, coupling to physics and application. Journal of Oceanography 58, 379–387.
García Lafuente, J., Criado Aldeanueva, F., 2001. La climatología y la topografía del Estrecho de Gibraltar determinantes de las propiedades termohalinas del agua del Mar Mediterráneo. Física de la Tierra 13, 43–54 (in Spanish).
García-Lafuente, J., Ruiz, J., 2007. The Gulf of Cádiz pelagic ecosystem. Progress in Oceanography 74 (2–3), 228–251.
García-Lafuente, J., Vargas Domínguez, J.M., 2003. Recent observations of the exchanged flows through the Strait of Gibraltar and their fluctuations at different time scales. Recent Research Development in Geophysics 5, 73–84.
García-Lafuente, J., Vargas, J.M., Plaza, F., Sarham, T., Candela, J., Basheck, B., 2000. Tide at the eastern section of the Strait of Gibraltar. Journal of Geophysical Research 105 (C6), 14197–14213.
García-Lafuente, J., Delgado, J., Vargas, J.M., Vargas, M., Plaza, F., Sarhan, T., 2002. Low frequency variability of the exchanged flows through the Strait of Gibraltar during CANIGO. Deep-Sea Research II 49 (19), 4051–4067.
Garrett, C., Bormans, M., Thompson, K., 1990. Is the exchange through the Strait of Gibraltar maximal or submaxima? The Physical Oceanography of Sea Straits. K.A. Publishers, pp. 271–294.
Gómez, F., Echevarría, F., García, C.M., Prieto, L., Ruíz, J., Reul, A., Jiménez-Gómez, F., Varela, M., 2000a. In: Microplankton distribution in the Strait of Gibraltar: coupling between organism and hydrodynamics structures. Journal of Plankton Research 22 (4), 603–617.
Gómez, F., González, N., Echevarría, F., García, C.M., 2000b. Distribution and fluxes of dissolved nutrients in the Strait of Gibraltar and its relationships to microphytoplankton biomass. Estuarine, Coastal and Shelf Science 51, 439–449.
Gómez, F., Gorsky, G., Striby, L., Vargas, J.M., Gónzalez, N., Picheral, M., García-Lafuente, J., Varela, M., Goutx, M., 2001. Small-scale temporal variations in biogeochemical features in the Strait of Gibraltar, Mediterranean side – the role of NACW and the interface oscillation. Journal of Marine Systems 30, 207–220.
Hopkins, T.S., 1999. The thermohaline forcing of the Gibraltar exchange. Journal of Marine Systems 20, 1–31.
Izquierdo, A., Tejedor, L., Sein, D.V., Backhaus, J.O., Brandt, P., Rubino, A., Kagan, B.A., 2001. Control variability and internal bore evolution in the Strait of Gibraltar: a 2-D two-layer model study. Estuarine, Coastal and Shelf Science 53, 637–651.
Kundu, P.K., 1990. Fluid Mechanics. Academic Press, 638 pp.
Lacombe, H., Richez, C., 1982. The regime of the Strait of Gibraltar. In: Elsevier Oceanography Series, vol. 34. J.C.J. Nilhoul.
Le Provost, C., Lyard, F., Molines, J.M., Genko, M.L., Rabilloud, F., 1998. A hydrodynamic ocean tide model improved by assimilating a satellite altimeter-derived data set. Journal of Geophysical Research 103, 5513–5529.
Macías, D., García, C.M., Echevarría, F., Vázquez-Escobar, A., Bruno, M., 2006. Tidal induced variability of mixing processes on Camarinal Sill (Strait of Gibraltar). A pulsating event. Journal of Marine Systems 60, 177–192.
Mercado, J.M., Cortés, D., García, A., Ramírez, T., 2007. Seasonal and inter-annual changes in the planktonic communities of the Northwest Alboran Sea (Mediterranean Sea). Progress in Oceanography 74 (2–3), 273–293.
Minas, H.J., Minas, M., 1993. Influence du Détroit de Gibraltar sue la biogéochime de la Méditerranée et du proceh Atlantique. Annales de L'Institute Océanographique 69, 203–214.
Minas, H.J., Coste, B., Le Corre, P., Minas, M., Raimbault, P., 1991. Biological and geochemical signatures associated with the water circulation through the Strait of Gibraltar and in the Western Alboran Sea. Journal of Geophysical Research 96 (C5), 8755–8771.
Navarro, G., 2004. Escalas de variación espacio-temporal de procesos pelágicos en el Golfo de Cádiz. Ph.D. Thesis, University of Cádiz, Cádiz, Spain, unpublished.
Osborne, T.R., 1980. Estimates of the local rate of vertical diffusion from dissipation measurements. Journal of Physical Oceanography 10, 83–89.
Packard, T.T., Minas, H.J., Coste, B., Martinez, R., Bonin, M.C., Gostan, J., Garfield, P., Christensen, J., Dortch, Q., Minas, M., Copin-Montegut, G., Copin-Montegut, C., 1988. Formation of the Alboran oxygen minimum zone. Deep-Sea Research 35 (7), 1111–1118.
Peltier, W.R., Caulfield, C.P., 2003. Mixing efficiency in stratified shear flows. Annual Review Fluid Mechanical 35, 135–167.
Pettigrew, N.R., 1989. Direct measurements of the flow of western Mediterranean deep water over the Gibraltar Sill. Journal of Geophysical Research 94 (C12), 18089–18093.
Redfield, A.C., Ketchum, B.H., Richards, F.A., 1963. The influence of organisms on the composition of seawater. In: Hill, M.N. (Ed.), The Sea. W. Interscience, New York.
Reul, A., Vargas, J.M., Jiménez-Gómez, F., Echevarría, F., García-Lafuente, J., Rodriguez, J., 2002. Exchange of planktonic biomass through the Strait of Gibraltar in late summer conditions. Deep-Sea Research II 49, 4131–4144.
Ruiz, J., Echevarría, F., Font, J., Ruiz, S., García, E., Blanco, J.M., Jiménez-Gómez, F., Prieto, L., González-Alaminos, A., García, C.M., Cipollini, P., Snaith, H., Bartual, A., Reul, A., Rodríguez, V., 2001. Surface distribution of chlorophyll, particles and gelbstoff in the Atlantic jet of the Alborán Sea: from submesoscale to subinertial scales of variability. Journal of Marine Systems 29, 277–292.
Sannino, G., Bargagli, A., Artale, V., 2002. Numerical model of the mean exchange through the Strait of Gibraltar. Journal of Geophysical Research 107, 3044–3057.

Sannino, G., Bargagli, A., Artale, V., 2004. Numerical modeling of the semidiurnal tidal exchange through the Strait of Gibraltar. Journal of Geophysical Research 109 (C050).

Sein, D.V., Backhaus, J.O., Brandt, P., Izquierdo, A., Kagan, B.A., Rubino, A., Tejedor, L., 1998. Flow exchange and tidally induced dynamics in the Strait of Gibraltar as derived from a two-layer, boundary-fitted coordinated model. In: Unesco Workshop on Oceanic Fronts and Related Phenomena, unpublished.

Smolarkiewicz, P.K., Margolin, L.G., 1998. MPDATA: A finite-difference solver for geophysical flows. Journal of Computational Physics 140 (2), 459–480.

Tsimplis, M.N., Bryden, H.L., 2000. Estimation of the transports through the Strait of Gibraltar. Deep-Sea Research I 47, 2219–2242.

van Genn, A., Rosener, P., Boyle, E., 1988. Entrainment of trace-metal-enriched-Atlantic-shelf water in the inflow to the Mediterranean Sea. Nature 331, 423–426.

Vargas, J.M., García Lafuente, J., Candela, J., Sánchez, J.A., 2006. Fortnightly and monthly variability of the exchange through the Strait of Gibraltar. Progress in Oceanography 70 (2–4), 466–485.

Wang, D.P., 1989. Model of mean and tidal flows in the Strait of Gibraltar. Deep-Sea Research 36 (10), 1535–1548.

Wang, D.P., 1993. The Strait of Gibraltar model: internal tide, diurnal inequality and fortnightly modulations. Deep-Sea Research I 40A, 1187–1203.

Wesson, J.C., Gregg, M.C., 1994. Mixing at Camarinal Sill in the Strait of Gibraltar. Journal of Geophysical Research 99 (C5), 9847–9878.

Wu, P., Haines, K., 1996. Modelling the dispersal of Levantine Intermediate Water and its role in Mediterranean deep water formation. Journal of Geophysical Research 101 (C3), 6591–6607.